DOI: 10.13009/EUCASS2023-687
Aerospace Europe Conference 2023 – 10TH EUCASS – 9TH CEAS

Advanced RNP Helicopter Procedure and Instrument Flight Procedure Design

*Heinz Wipf**
** AIRNAVCONSULTING GmbH*
H-8008 Zurich Switzerland
airnavconsulting@bluewin.ch

Abstract

Data analytical results gathered in flight trials in the course of introducing Performance Based Navigation (PBN) are shown. Switzerland has extensively researched and probed into Instrument Flight Rules (IFR) helicopter operations. This resulted in performance bounds beyond OEM-certified limits. Light helicopters have limited capability to carry extensive avionics because to other mission critical on-board equipment. Operational scenarios however include all-weather capability. The flight trials with an on board mounted flight calibration equipment for helicopters had, among other objectives the gathering of the lateral (cross track) Navigation System Error (NSE) and Total System Error (TSE) of an auto-piloted light helicopter. The helicopter navigates with only GPS/SBAS L1 C/A NAV. The OEM certified it for RNP0.3. Besides navigation errors and its correlation indications of instrument flight procedure design for low RNP values is illustrated.

1. Introduction

When introducing PBN in Switzerland a considerable portion of the program was directed towards instrument flight rules (IFR) helicopter operations. Light helicopters in use for disaster relief, SAR and emergency medical services operated by private or state authorities show limited capability to carry extensive avionics due to the weight of other mission critical on-board equipment. With the necessity of an ever-widening operational scenario, all-weather capability becomes a key element in specific helicopter operations. The use of GNSS as a primary navigation source is therefor an obvious choice. Commencing to fly advanced IFR procedures in demanding mountainous terrain SBAS quickly became the GPS augmentation of choice. As a consequence the navigation total system error (TSE) was reduced significantly.
At the same time ICAO's IFPP[1] started to look closer into IFR helicopter procedures and its lateral buffer values derived from the design of fixed wing aircraft procedures [2]. These to be applied buffer values must of course be related to the probability density functions of helicopter TSE.
Procedure designers typically use lateral buffers to avoid controlled flight into terrain (CFIT). But such buffers consume airspace that either is not in existence[2] or is to be used for other air traffic.[3] These buffers are based on fairly old empirical data.[4]
Apparently empirical TSE data sets are globally in short supply. Getting notice from the IFPP, we set out to collect this data as part of PBN helicopter flight trials in the Swiss Alps. Apart from data collecting we also undertook the necessary steps in data analysis. Thereby outliers in the statistical data sets were discovered. These outliers have for many years spurred discussions about the tails of probability density functions and their parameters. Given the data sets acquired during the helicopter flight trials[5], hypothesis and possible explications for the outliers are discussed.
Any flight path s can be described as a mass point's trajectory in three dimensions x, y, z, that is $\in R^3$. The mass point is typically located at the aircraft's center of gravity.

$$x = f\langle t\rangle, y = f\langle t\rangle, z = f\langle t\rangle \tag{1}$$

[1] Instrument Flight Procedure Panel
[2] E.g. terrain, alpine canyons
[3] Military
[4] Collision Risk Modeling (CRM) - ICAO Doc 9274-AN/904 1st Edition 1980
[5] All fights were operated in VMC under IFR in airspaces with no ground based navigation means. Other trial objectives were the helicopter's FMS/AP capability to fly RNP0.1 AR APCH, RF intermediate segments and LPV - PinS APCH and DEP

DOI: 10.13009/EUCASS2023-687

where

$$ds\langle t\rangle = \left(dx\langle t\rangle^2 + dy\langle t\rangle^2 + dz\langle t\rangle^2\right)^{\frac{1}{2}} \tag{2}$$

$$s\langle t\rangle = \int \left(dx\langle t\rangle^2 + dy\langle t\rangle^2 + dz\langle t\rangle^2\right)^{\frac{1}{2}} dt \tag{3}$$

The physical laws governing such a trajectory have been described by Newton, namely his second law of motion.

$$\vec{F} = m \cdot \vec{a}\langle t\rangle = m \cdot \frac{d}{dt}\vec{v}\langle t\rangle = m \cdot \frac{d^2}{dt^2}\vec{s}\langle t\rangle \tag{4}$$

Where F is the force exercised on the airframe, m is the mass of the aircraft and a is the acceleration, v the speed and s the trajectory of the aircraft. For the sake of simplicity let R^3 be reduced to R^2 and $s\langle t\rangle$ split up in its orthogonal components $x\langle t\rangle$ and $y\langle t\rangle$.[6] The problem to solve thus is to find a class of trajectories or 3d curves for which the curvature is a polynomial function of the length $s\langle t\rangle$. A cost function in discussion for helicopters is the altitude, which of course is governed by the minimum height above terrain.

2. Analytical considerations

Today's flight procedure design suggests curved flight trajectories, especially for advanced approach and departure (APCH and DEP). The standardized design is called Radius-to-Fix (RF), whereas a straight-line segment is connected to another segment being part of a circle circumference defined by its radius and the coordinates of the start and end waypoint or fix. The coding of the flight management system (FMS) is done in a likewise fashion. While civil engineers in railroads (late 19th century) and later in highway construction (middle of 20th century) have applied physical curves for some time [8], aviation has obviously not felt the necessity to do so. The fact is that a straight segment interfacing a circle segment in a tangent fashion has no second derivative of $s\langle t$.[7] In consequence to Newton's 2nd law the accelerations is undefined. The author discovered this shortcoming in instrument procedure design at a PBN workshop back in 2009 for the first time, while other authors [7 p 3] addressed it already in 2006.

Helicopters [9 p 162, 177] and modern jet fighters are inherently unstable - a feature which typically supports the aircraft's agility in flight. Simple damping would therefor impair the responsiveness of the auto-piloted aircraft and is therefor no viable option. The instability makes those aircraft the platform of choice to study the response due to sudden abrupt autopilot commands. The abrupt reaction of a helicopter in flight is clearly discernible while passing a fix, which joins a straight leg with a circular turn. Albeit the difference in flight dynamics, a stable fixed wing aircraft will eventually perform a smoother flight[8]. The resulting error in the flight path will be locally of a lesser magnitude but will persist for a longer interval before and after the fix.

Analysing the situation, calculus is of no help, because an analytical solution is not possible and there is a mathematical proof for it. Yet it is possible to apply a trick to approximate the effect such a transition has on the acceleration of a mass point. The trajectories can be discretized in time. Hence double differentiation of $s\langle t\rangle$ can be applied. This results in an approximation of the acceleration (right graphics) to which the mass point is subjected to while trying to follow one of the typical trajectories (left graphics) below.

[6] The problem space remains in R^3 as can be seen from the mathematical notation, as t is a parameter and not an additional dimension.
[7] "The transition from a straight line to a circular arc is always abrupt, even if this is not readily noticeable at very large radii or low travel speeds.." translated from [8 p 1.
[8] See so called 'turn anticipation'

DOI: 10.13009/EUCASS2023-687

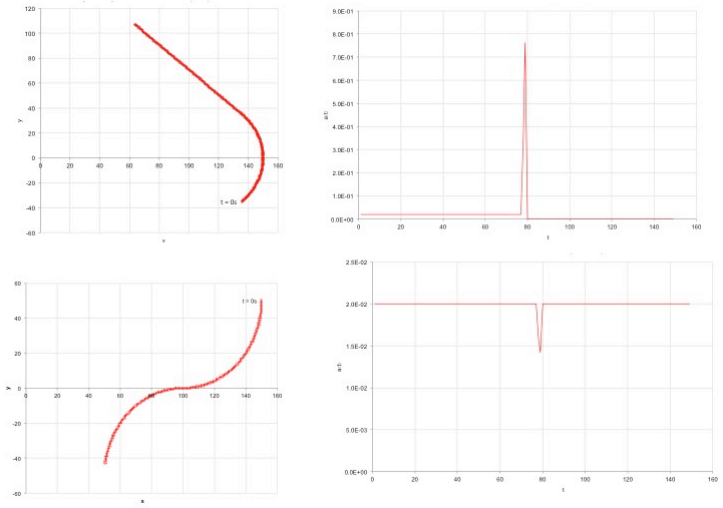

Figure 1 – Discrete double differencing of a radius-to-fix and a radius-to-radius transition.

3. Procedures

The flight trials in the Swiss Alps were planned at 1800mMSL and above. All trajectory design followed RF as described above.
The flight guidance had to be based on GNSS/SBAS. All flights were planned to operate in VMC[9] under IFR and in airspaces with no ground based navigation means. The chart in **Figure 2** covers an exemplary part of the trajectories flown during those trials. The approach procedure for RWY 21 LSZS is not shown to avoid clutter, but is referenced under [5].
A detail of importance for the sequel is that the trajectory flown consisted of RF and straight legs as described in **Figure 1**.

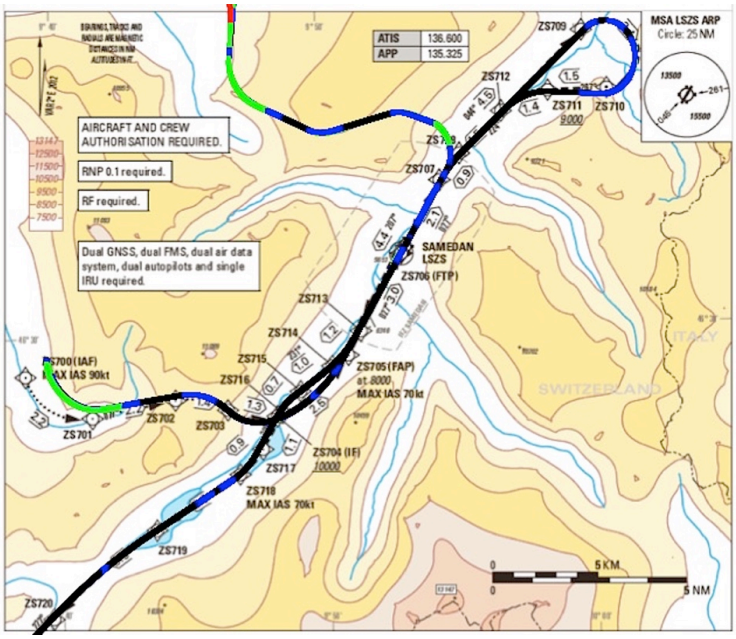

Figure 2 - Procedure chart SAMEDAN LSZS RWY03 [4] - all runs (nr2…nr9) superposed as overlay with their cross track TSE color-coded. |rnavCrossTSE| > 100m, > 30m, > 10m, < 10m.

[9] Visual meteorological conditions

DOI: 10.13009/EUCASS2023-687

It is noticeable 95% of all |rnavCrossTSE| values were < 36.37m or < 0.0196nm, which would suffice for RNP0.02 - at least empirically.

4. Flight trials

The flight trial program for the implementation of the helicopter procedure SAMEDAN LSZS RNAV (RNP) RWY 03/21 HELICOPTER CAT H in 21.04.2016 also comprised a helicopter flight inspection and flight validation. Other trial objectives were the helicopter's FMS/AP capability to fly RNP0.1 AR APCH, RF intermediate segments and LPV - PinS[10] APCH and DEP. Other objectives were the gathering of empirical lateral (cross track) Navigation System Error (NSE) and Total System Error (TSE) of an auto-piloted light helicopter with only one kind of NAV sensor (GNSS/SBAS). The flight trials themselves were part of the European PBN Rotorcraft Operations under Demonstration project (PROuD).[11]
The aircraft flown was a Rega AW109SP. The helicopter is IFR certified and its avionic suite features two primary GNSS receivers and is certified for LPV, LNAV/VNAV and LNAV. The flight characteristics state a minimum speed of 55kt if flown under autopilot and IFR, while under LPV one is allowed to reduce to 45kt with a LNAV/VNAV or LPV glide path angel of 9 degrees. With the autopilot engaged the maximum bank angle is of v/10 + 7 v in kt. This results in 120kt: 19°, 90kt: 16°, 70kt: 14° (see also Fig. 9). The minimum turn radius is 800ft and 360° in 2 min which equals $3°s^{-1}$.
The flight check used the specifically developed inspection system HeliFIS by Aerodata. The system records among other data all relevant parameters of the GNSS/SBAS[12] signals. The recordings permit a post flight ASCII data extraction. Flight data from the FMS and primary GPS were recorded on board the aircraft with help of fixed installed quick access recorder[13]. For a complete list of processed variables is available with the author. A detailed review on the equipment and its aircraft integration is found in [3]. The meteorological condition has relevance to the trials in as far as the flights had to be conducted under VMC. Adverse wind conditions especially gusty cross winds could have had an uncontrolled impact on the navigation performance of the helicopter. However the flight meteorological data[14] for the day showed no noteworthy circumstances.

5. Data analysis

One general issue in test planning was the aspect in lateral or cross track navigation error evaluation. All runs where flown by the 4-axis autopilot. However not all runs from 1…9 were taken into account. Run nr1 had to be abolished due to a pilot intervention and runs nr8 and nr9 where outside of the trial scope. Nevertheless they are incorporated for completeness in some of the figures below. The data sets comprise 90020 positions sampled as time series along the trajectories of uneven lengths. The basic information on the data sets is summarized in **Table 1**. The TSO GPS receiver's covariance matrix provides data for evaluating the navigation system error (NSE) has a $1s^{-1}$ sampling rate while the HeliFIS calculates the position at $10s^{-1}$ for the total system error (TSE). This fact leads to NA's[15] in the navigation system error (NSE) data entry and explains the differences in sample size in the table.

Table 1 – Sample sizes and proportion of the different runs total

Run		**nr2**	**nr3**	**nr4**	**nr5**	**nr6**	**nr7**	**nr8**	**nr9**	**total**
TSE	Samples	4090	19917	5154	12821	11758	5400	7618	23262	**90020**
	Proportion	5%	22%	6%	14%	13%	6%	8%	26%	100%
NSE	Samples	496	2063	600	1363	1257	621	843	2407	**9650**
	Proportion	5%	21%	6%	14%	13%	6%	9%	25%	100%

The TSO GPS receiver providing data for evaluating the NSE has a $1s^{-1}$ sampling rate while the HeliFIS calculates the position at $10s^{-1}$ for the TSE.
Figure 3 presents the individual lateral TSE results for runs 2 through 9 as time series. The horizontal axis units are tenths of a second; the vertical axis units are meters of the lateral TSE. The time series exhibit a tendency of a progressive reduction of the lateral TSE as a function of time or along the trajectory. This effect has been brought to

[10] See ICAO publications for the different procedures
[11] See EU-report for further details. Refer to the PROuD SESAR Joint Undertaking. Demonstration Report (B1) 2016 LSD.02.09
[12] GPS and EGNOS
[13] Avionica miniQAR MKIII
[14] Winds in the valley were between 0 and 14kt and between 160° to 220°.METAR - Courtesy of Meteo Suisse
[15] NA for Not Available

DOI: 10.13009/EUCASS2023-687

the attention of the OEM. This behaviour was already visible in the first series of flight trials in 2015. The recordings for run nr8 and nr9 have a problem just right at the start, which renders the statistical analysis difficult. They are part of a different set and do not belong to this series of flight trials.[16] As a consequence of the comments in the footnotes, runs nr8 and nr9 have been removed in the sequel of this paper.

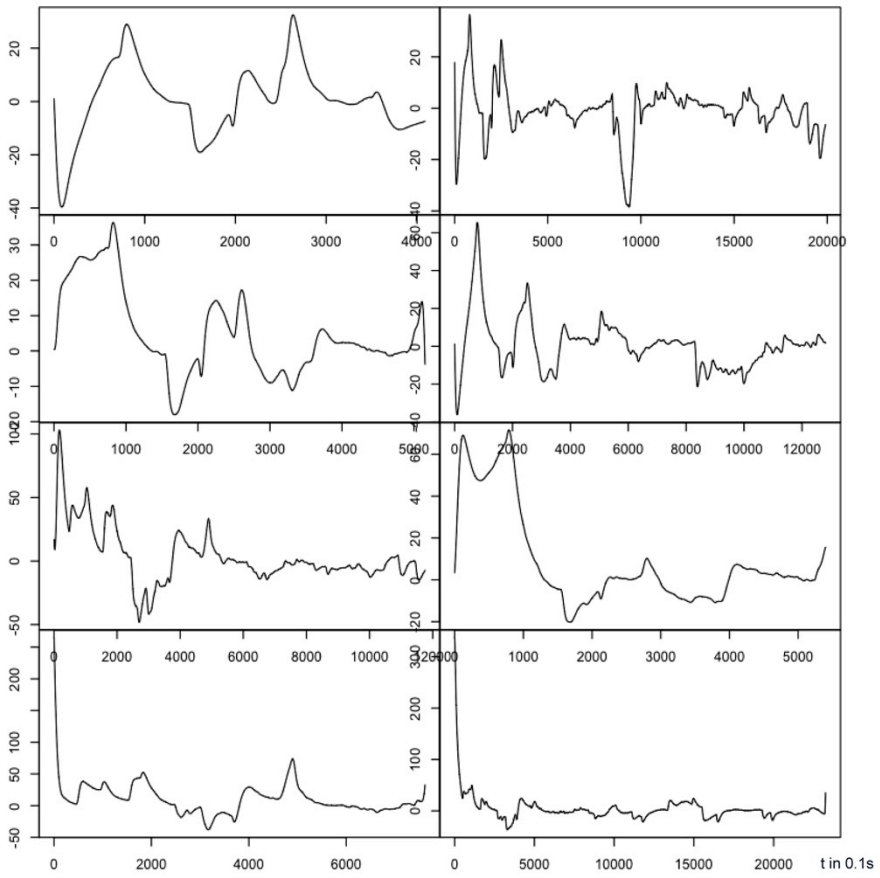

Figure 3 – Overview of the TSE on all runs (nr2 - nr9) on record from top left to right as time series.

Figure 4 displays the empirical probability densities of the lateral TSE for each of the individual relevant trial runs.

[16] The flight technical view confirms that the deviation at waypoint ZS780 may have an explanation in the short intercept in combination with its fly-by coding. Moreover the leg before ZS780 has not been defined yet. It is therefore not clear under which angle one should approach the waypoint - Ref. private communication 30.05.2016 pilot T. Gnägi/Rega -

DOI: 10.13009/EUCASS2023-687

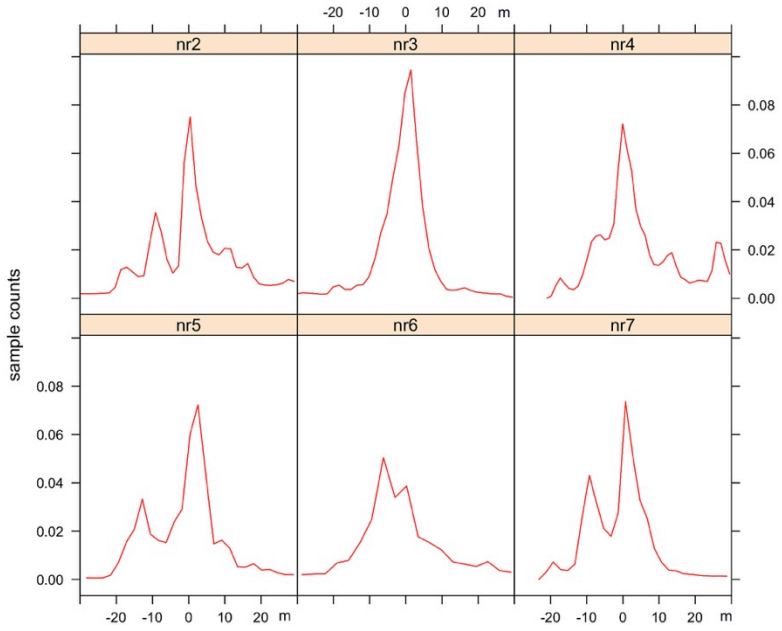

Figure 4 – Empirical densities in m^{-1} (y- axis) of the lateral TSE in m (x- axis)

The majority of the empirical distributions compare well with the theoretical graphs shown in **Figure 5**.

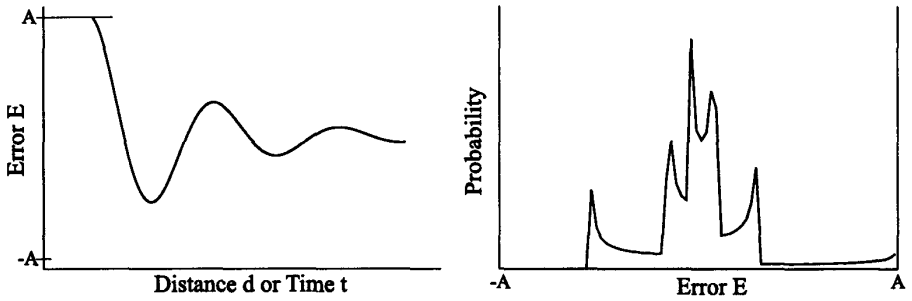

(a) (b)

Figure 5 –Theoretical error distributions b) resulting from the interaction of the control loop typically employed in an autopilot. Courtesy Dr. M. Scaramuzza[17]

Due to the second order control loops[18] generally employed in autopilot applications [10 p 366], it must be underlined that an individual flight trajectory has the tendency to exhibit a bi-modal U-shaped probability density function (pdf) representing lateral errors along the flight trajectory. This effect is visible in **Figure 4** nr2, 4, 5, 7 and to a lesser degree in nr6. The densities resemble the ones derived in [6 p 28].[19] For a more indebt view [11 p 436, 442 and 11] provide an overview and mathematical treatise of general flight control systems.
Fig. 5 shows boxplots for all 8 runs (nr2 - nr 9). In (a) with outliers and (b) with the outliers removed. Outliers are marked with small circles above and below the whiskers. The vertical axis is the rnavCrossTSE in m. Box sizes are in proportion to the square root of the sample size for the respective run and comprise 50% of the data. The horizontal bar in the box marks the median value of the sample set. The whiskers above and below the box extend to the extremes.

[17] From [6 p 30 Fig. 3.10]
[18] Private communication, Dr. A. Smerlas Certification Directorate - EASA
[19] Fig. 3.8, 3.9 and 3.10

DOI: 10.13009/EUCASS2023-687

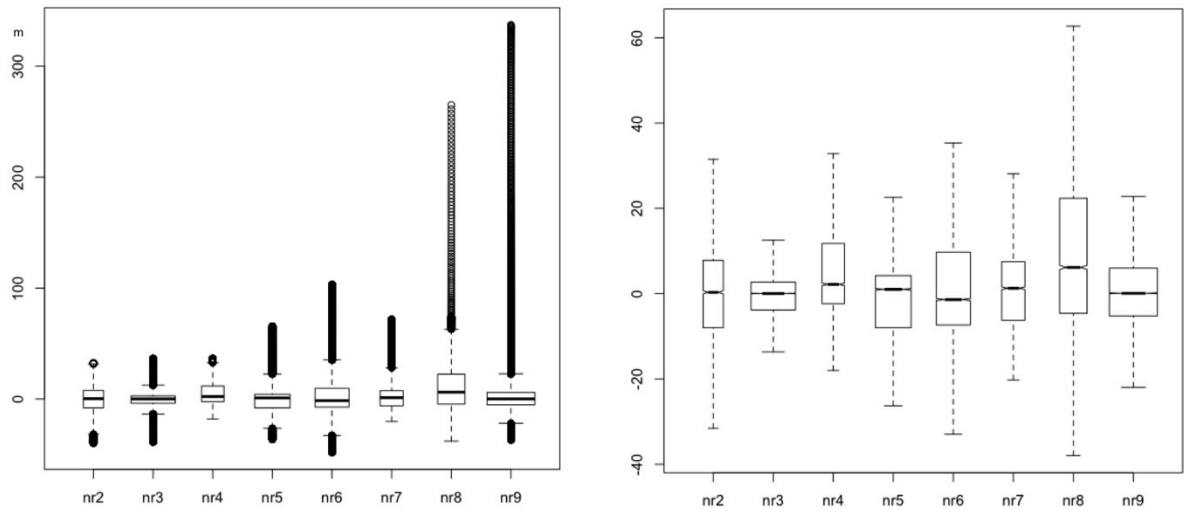

a) b)

Figure 6 - Boxplots all 8 runs (nr2 - nr 9) with outliers (a) and outliers graphically suppressed (b) y-axis in m.

All runs recorded outliers. With the exception of run nr3 the outliers were found to be asymmetrically distributed. This is also reflected in the skewed histogram and distribution in **Figure 7**. Again runs nr8 and nr9 display the largest outliers, which is due to the initial excursions shown in **Figure 3**. The boxplots from errors would typically rather look like Fig 4 b).

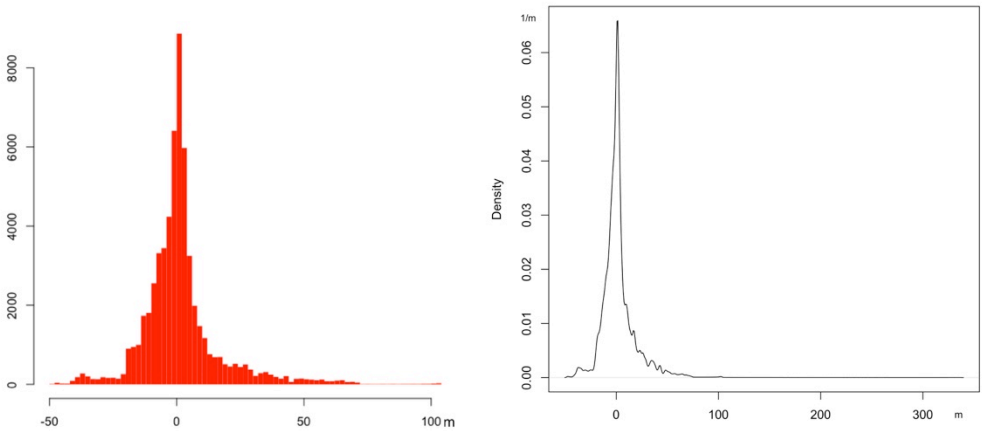

Figure 7 - The pooled data histogram comprising 59140 observations and the corresponding probability density in m^{-1} of runs nr2 ... nr7 showing the cross track TSE (bandwidth 0.7763 - Gaussian kernel).

The histogram and the distribution show the often-cited fat tails. Unlike the individual runs the pooled data now shows a mono-modal distribution, which is a result of the central limit theorem. But is the data Gaussian distributed?

DOI: 10.13009/EUCASS2023-687

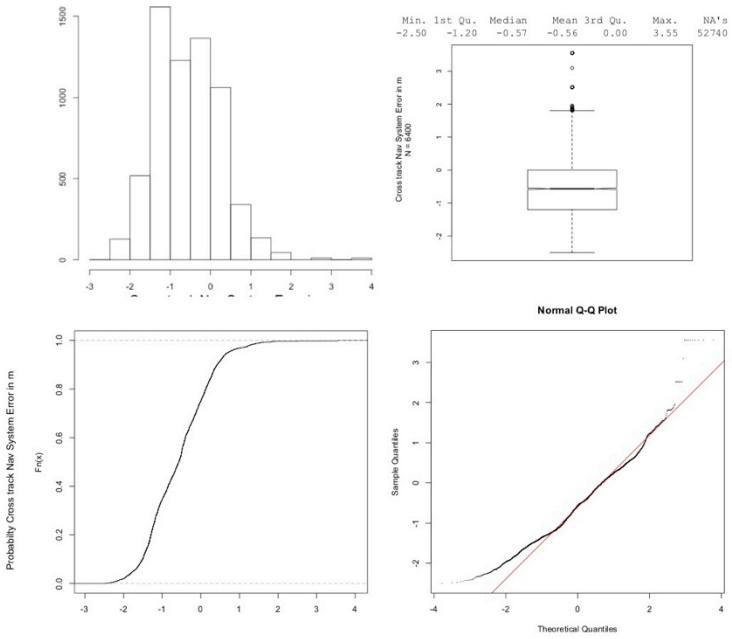

Figure 8 – NSE summary graphs and values of the pooled runs nr2 – nr7

The NSE shows a slight bias in the histogram. The GNSS sensor's performance under SBAS, while flying approach procedures in an alpine valley is rather remarkable,[20] remembering the helicopter is certified only to RNP1. Just a few outliers in the boxplot are observed. In appreciating the Q-Q plot[21] red line are the theoretical Gaussian distributed quantiles and the black dots the empirical data. The plot would allow assuming a normal distribution of the NSE. This is in accordance with the theory for space based radio signals. Despite the fact that the NSE data failed a statistical test[22] for normality, but for the sake of argument, let the empirical cumulating distribution function to the lower left of **Figure 8** be replaced with the theoretical normal distribution.
The parameters (mean⟨rnavCrossNSE⟩ = -0.564m and std⟨rnavCrossNSE⟩ = 0.805m) are estimated from the data set. This allows the probability estimation of the sensor errors.[23]

$$p = \int_{scross}^{\infty} \frac{1}{\sqrt{2\pi \cdot \sigma}} \cdot e^{\left(\frac{scross-\mu}{\sigma}\right)^2} d\, s_{cross} \tag{5}$$

Then the probability in having a navigation sensor offset laterally of > 5m would then be p = 2.4E-12.
A rather different situation is found in **Figure 9** with the TSE. Although the helicopter reaches 31m for 95% of the time the distributions do not render to the assumption of normality. This is clearly visible in the Q-Q plot to the lower right.

[20] Nr of satellites in view: 8 < tracked SV < 13 - the count includes 2 EGNOS SV
[21] Quartile-Quartile plot
[22] Shapiro-Wilk test of normality
[23] Error function erf

DOI: 10.13009/EUCASS2023-687

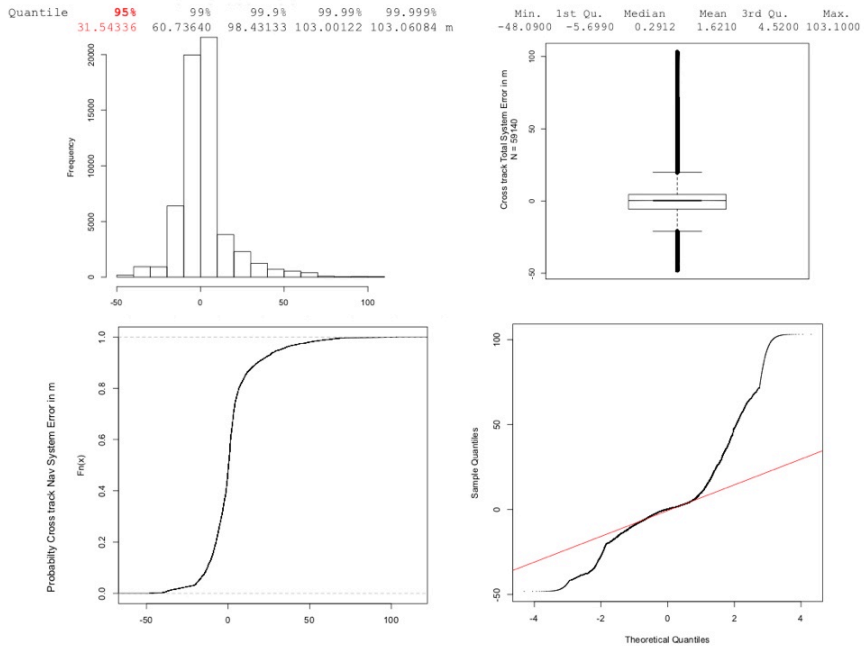

Figure 9 - TSE summary graphs and values of the runs nr2 – nr7

What then are the causes of the skewed empirical probability densities and the countless outliers in the TSE data? The navigation sensor knows the position of the aircraft fairly accurately.
The first point may be attributed to the non-existence of a balanced test plan, resulting in a non-equal distribution of the different transition combination.

Table 2 Transition combinations of flight segments from runs nr2 – nr7.

Apch'ing	Straight Seg	RF left	RF right
Straight Seg	NA	11	16
RF left	22	6	0
RF right	11	5	0

The transitions in **Table 2** are derived from the recorded heading information.
A second consideration is contained in the **Figure 10**. It is exhibiting pairwise scatter plots. The Spearman correlation coefficient[24] including p-values for the statistical test of the correlation between different variables for runs nr2 – nr7 are given. Units on vertical and horizontal axis are in m with the exception of the pitch/bank angles, which are in degrees. The green line on the scatter plots is the result of a local polynomial regression fitting (Loess). One may observe the correlation coefficient of r = 0.44 between bank angle and TSE, which gives rise to the hypothesis that the TSE may be related to turns of the helicopter. The navigation system error stays unaffected and does not correlate with the bank angle. This negates the possibility that masking of GPS space vehicles (SV) in the mountain valley would be the cause of the TSE[25]. This hypothesis is further supported by the fact of a missing correlation between the pitch and the NSE. In addition the pitch also seems to have no impact on the TSE only the bank angle does. It should be noted that most p-values show low values, so that H_0 can be rejected and H_A[26] holds on a 0.05 basis with the only exception in the case of TSE and NSE. The flat slope of the regression line reflects the correlation. This also means that a influence of the rnavCrossNSE to the rnavCrossTSE cannot be too important. Since the probability density TSE is a convolution of the NSE and the FTE. As a result the FTE seems to predominantly determine the TSE.

[24] The Spearman correlation coefficient has been chosen for its robustness towards outliers as encountered in the data sets at hand and because the data must not necessarily come from bivariate normal distribution.
[25] 8 < nr of tracked SV's < 13 - the count includes 2 SV's EGNOS
[26] H_A: The true r is not equal to 0 – two-sided test

DOI: 10.13009/EUCASS2023-687

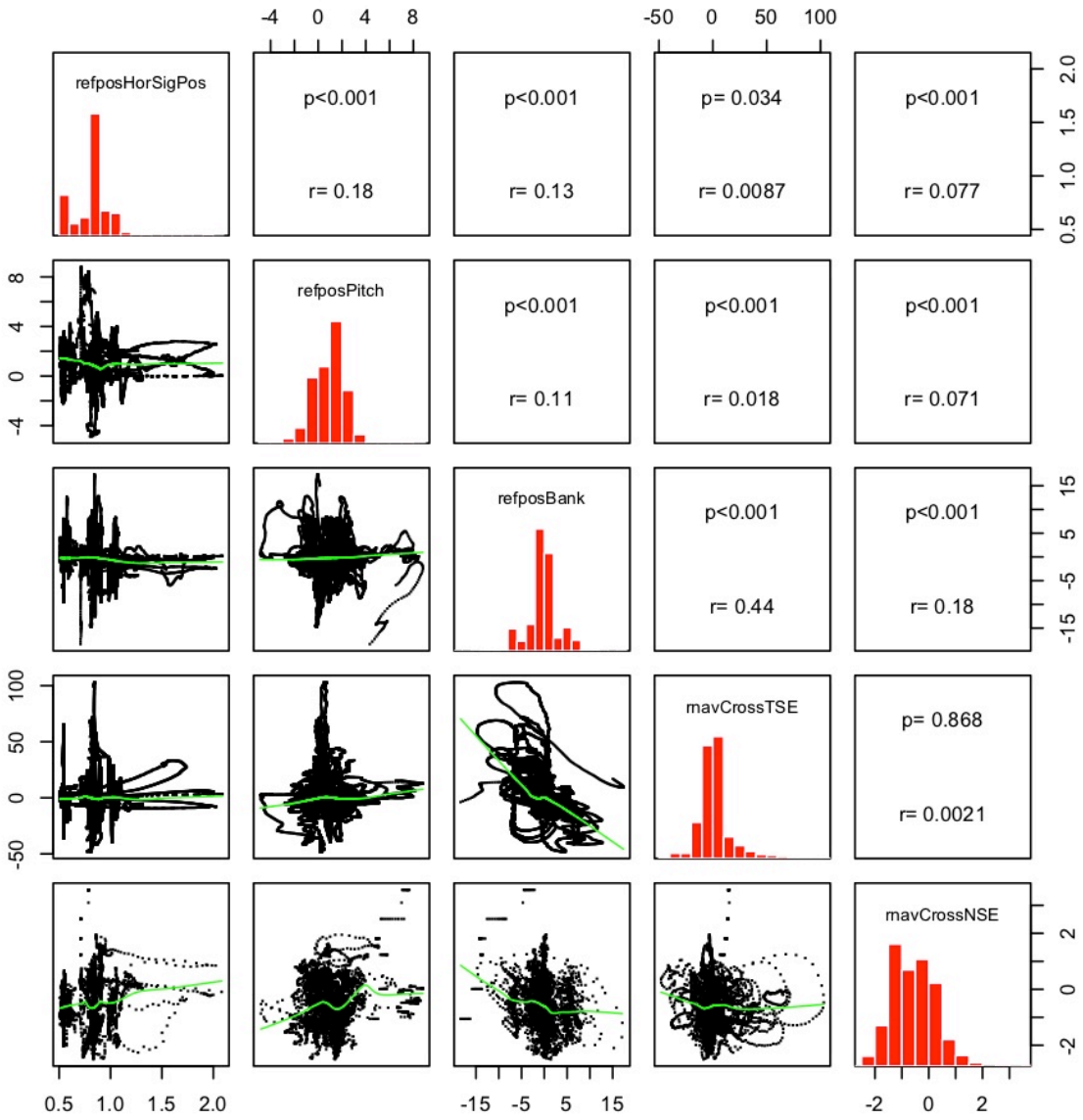

Figure 10 - Pairwise scatter plots with the correlation coefficient between the different variables and univariate histograms.

The time series of the cross track TSE is transformed in showing the distance on the x-axis and the 1st differences (viz the cross track velocity) on the y-axis. Furthermore the distance from fix to fix (ZS70.) were extracted from the procedure charts in **Figure 2** and displayed on the upper x-axis.

Since **Figure 11** is exemplary for all runs it clearly shows the systematic impact the various transitions have on the cross track TSE. The cross track TSE acceleration needs a double differentiation, which evidently increases the noise (**Figure 12**). For comparison the cross track acceleration of the flight technical error FTE is displayed in **Figure 13**.

Clearly if operators fly in an RNP2 environment[27] these effects will hardly be discernible. But EMS[28], SAR[29] or other logistic helicopter IFR operations in obstacle rich environments and demanding terrain, precision flying down to RNP0.1/0.05 matters.

The author is of the opinion that properly equipped light helicopters are capable of a much more exigent navigation performance under IFR then that for which they are certified today. This however assumes that the trajectories of the procedures are devised in accordance with the laws of physics [1].

[27] Required navigation performance: 2 NM cross track error for 95% of the flight time
[28] Emergency medical service
[29] Search and rescue

DOI: 10.13009/EUCASS2023-687

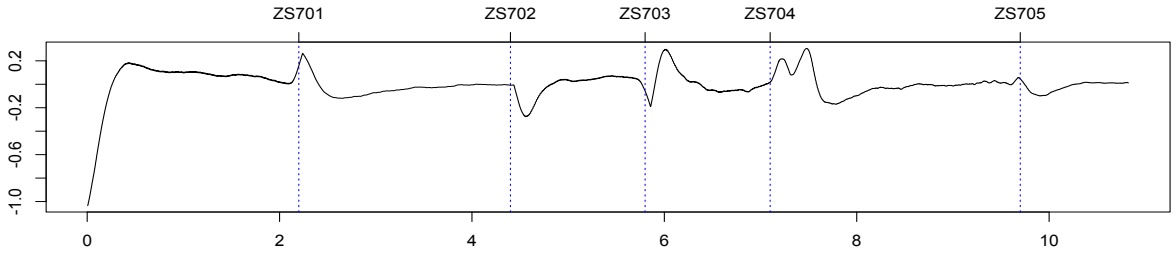

Figure 11 – Run nr2 TSE cross track velocity (y-axis m/0.1s x-axis NM) sample interval 0.1s.

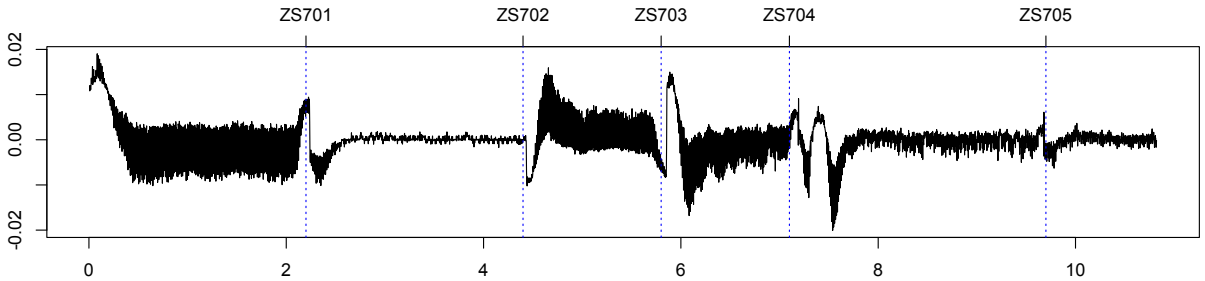

Figure 12 – Run nr2 TSE cross track acceleration (y-axis m/0.01s^2 x-axis NM)) sample interval 0.1s.

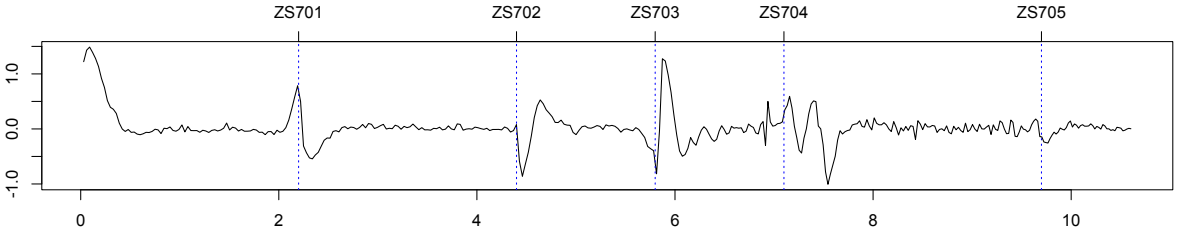

Figure 13 – Run nr2 FTE cross track acceleration (y-axis m/s^2 x-axis NM)) sample interval 1s.

6. Conclusion

The lateral GNSS based NSE of aircraft over the years is decreasing and with it the TSE. This fact is useful for the design of advanced IFR flight procedures and to estimate the collision probability with cross track obstacles or terrain. However whether a flight track is devised as a polygon from fix to fix or a more sophisticated radius-to-fix, such trajectories are non-physical. For 1st and 2nd time derivative must exist for a point mass to follow it in theory. A fact, considering Newton's 2nd law, obviously not fulfilled under today's instrument flight procedure design rules. This also shows in an additional statistical protection measure, called path definition error (PDE) [12 § 2.2.2.2]. An error source unnecessary if a physical trajectory [7] was applied. Literature shows there are neither highways nor high-speed railroad tracks today that have such non-physical layouts [8]. It seems also unclear whether the lateral deviations from the trajectory (TSE) and the therefore necessary buffers have to protect a single flight or all flights passing a certain critical or governing obstacle, both having seemingly different lateral probability distributions (**Figure 4**, **Figure 7**). The pilot is obviously concerned with the first one while an airport or an air navigation service provider interests the latter.

The ICAO IFPP[30] strives to rationalize that the lateral buffers for advanced RNP-procedures. This must be supported by empirical data in much the same way the CRM[31] has been established in the past. The point in question is a parametric probability density function that went through a statistical test. To derive parametric densities the empirical data sets have to be free of systematic errors like the ones stemming from a non-physical trajectory design

[30] Instrument Flight Procedure Panel
[31] Manual on the Use of the Collision Risk Model for ILS Operations DOC9274-AN/904 1980

DOI: 10.13009/EUCASS2023-687

as shown in this paper. A possible way forward is to devise trajectories based on curves having a 1st and 2nd derivative in time.
There are a number of candidate functions like simple polynomials, clothoids [8], Bezier curves[32] or different splines[33] to approximate a flight trajectory, while at the same instant satisfy 1st and 2nd derivatives. The problem for FMS data coders and packers of the procedures would then be, how to discretize the analytical function received from the designer. An example of a trajectory generation process is to be found in [7 p 4].
Enough data to form empirical density functions would also do, but to get hold of the distribution tails the volume of data is considerable. Given the observed enthusiasm demonstrated up until today in providing this empirical data, this endeavour seems to be elusive. Whether resampling techniques such as the bootstrap and jackknife provide a way out of having insufficient empirical data remains to be analysed. Newer empirical data must undergo a comprehensive analysis, in order to test statistical hypothesis of given probability-density-functions and thus allow appropriate procedure design.

References

[1] Newton I. “Philosophiæ Naturalis Principia Mathematica” 1687
[2] WP 1c-001 First presented: 14-1 Instrument Flight Procedure Panel Working Group Meeting 14-1 WG 2 – Helicopters, Fukuoka, Japan March, 2017
[3] Schwendener et al “Flight Inspection of Helicopter Procedures in a Challenging Topographic Environment” IFIS 2014
[4] SAMEDAN LSZS RNAV (RNP) RWY 03 HELICOPTER CAT H 17.02.2017
[5] SAMEDAN LSZS RNAV (RNP) RWY 21 HELICOPTER CAT H 02.03.2017
[6] Scaramuzza M. "Systematic Investigations of Error- and System-Modelling of Satellite Based Flight Approaches and Landings in Switzerland" Diss. ETH No. 12892 Zurich 1998
[7] Smerlas A.J. et al “On the Development of a four-axis AFCS for the Pilot Assistance Experimental System” dspace-erf.nlr.nl 2006
[8] Bachmann E. “Die Klothoide als Übergangskurve im Straßenbau” Schweizerische Zeitschrift für Vermessung, Kulturtechnik und Photogrammetrie 1951 Band 49 Heft 6
[9] Saunders G. H. "Dynamics of Helicopter Flight" NY 1975
[10] Collinson R. P. G. "Introduction to Avionics" London UK. 1998
[11] Stengel R. "Flight Dynamics" Princeton 2004
[12] ICAO PBN Manual Doc 9613 of 2013

[32] After P. Bézier, at Rénault in early 1960 and in a similarly but unpublished work by P. de Casteljau at Citroen late 1950s and early 1960.
[33] I.J. Schoenberg in 1946

DOI: 10.13009/EUCASS2023-687

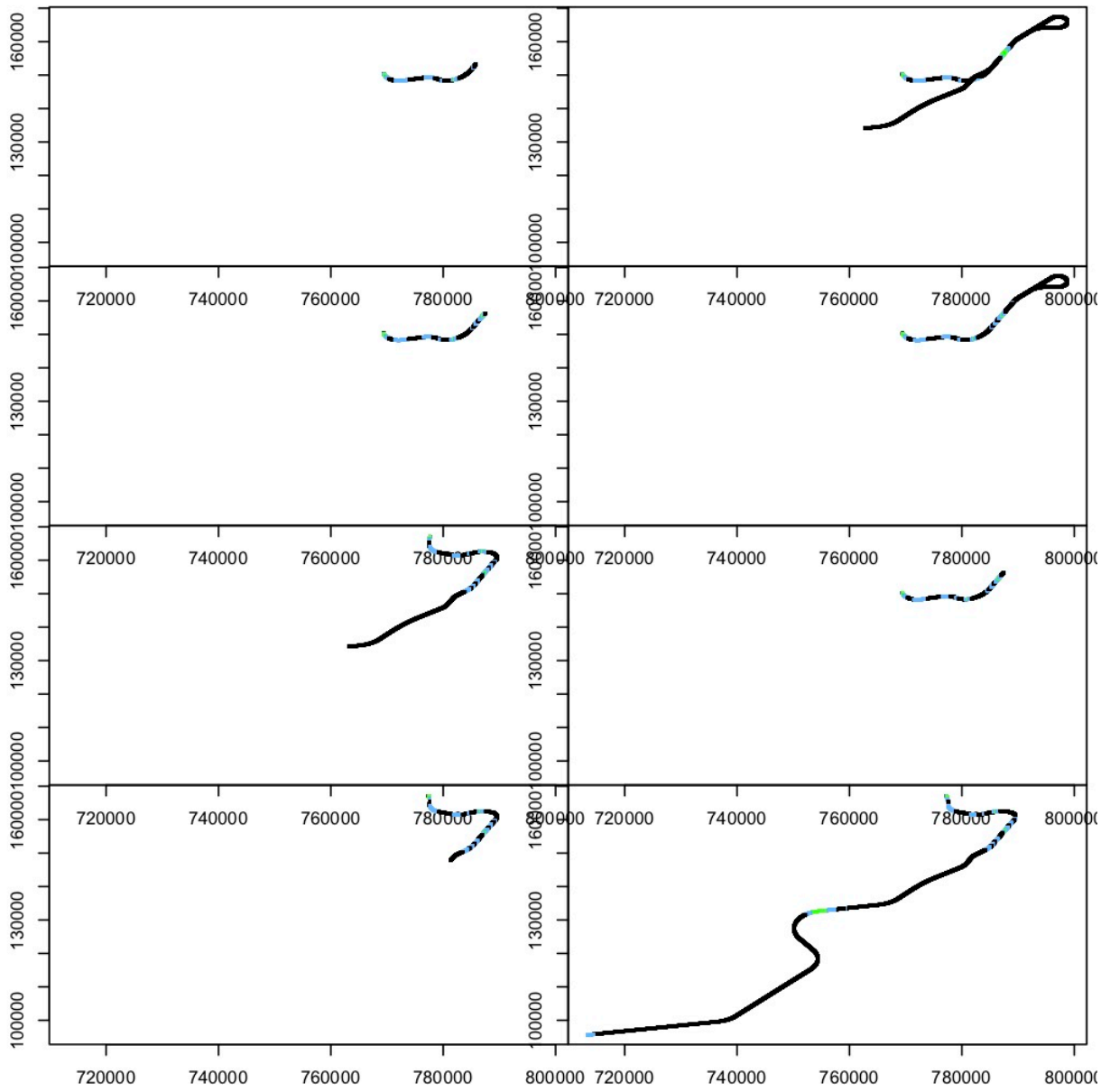

Overview of all runs (nr2 - nr9) on record from top left to right |rnavCrossTSE| = > 100m, > 30m, > 10m, < 10m.
The Y and X axis are virtual and in m